FOURIER-TRANSFORM INFRARED SPECTROSCOPY OF ETHYL LACTATE DECOMPOSITION AND THIN-FILM COATING IN A FILAMENTARY AND A GLOW DIELECTRIC BARRIER DISCHARGE

Natalia Milaniak[1,2,3], Gaétan Laroche[2,3], Françoise Massines[1]

[1] *Laboratoire PROcèdes Matériaux et Energie Solaire, UPR 8521, CNRS PROMES, Perpignan, France*

[2] *Laboratoire d'Ingénierie de Surface, Département de génie des mines, de la métallurgie et des matériaux, Centre de Recherche sur les Matériaux Avances, Université Laval, Québec, Québec, Canada*

[3] *Centre de recherche du CHU de Québec, Hôpital St. François d'Assise, Québec City, Québec, Canada*

Correspondence
Gaétan Laroche, Laboratoire d'Ingénierie de Surface, Département de génie des mines, de la métallurgie et des matériaux, Centre de Recherche sur les Matériaux Avances, Université Laval, 1045, Ave de la Médicine, Québec G1V 0A6, Québec, Canada.
Email: Gaetan.Laroche@gmn.ulaval.ca

Françoise Massines, CNRS PROMES, Laboratoire PROcèdes Matériaux et Energie Solaire, UPR 8521, Tecnosud, 66100 Perpignan, France.
Email: Francoise.Massines@univ-perp.fr

Funding information Natural Sciences and Engineering Research Council of Canada (GL); Agence Nationale de la Recherche (FM)

ABSTRACT

Glow and filamentary regimes of atmospheric pressure plasma-enhanced chemical vapor deposition in a planar dielectric barrier discharge configuration were compared for thin-film deposition from ethyl lactate (EL). EL decomposition in the plasma phase and thin-film composition were both characterized by Fourier- transform infrared spectroscopy. EL chemical bonds' concentration along the gas flow decreases progressively in the glow dielectric barrier discharge (GDBD), whereas it drastically oscillates in the filamentary dielectric barrier discharge (FDBD), with values higher than that of the initial mixture. EL decomposition route depends on the discharge regime, as the decrease of the concentration of the different investigated bonds is different for an identical amount of energy provided to EL molecules. CO_2 is systematically formed reaching concentrations of 25 and 40 ppm, respectively, in FDBD and GDBD.

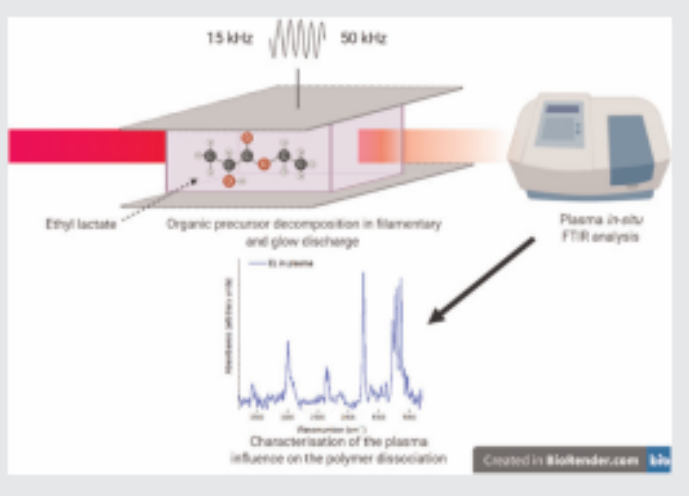

KEYWORDS
biomaterials, chemical composition, dielectric barrier discharge, FSK, FTIR, in situ spectroscopy, plasma, thin film

CITATION
N. Milaniak, G. Laroche, F. Massines. Fourier-transform infrared spectroscopy of ethyl lactate decomposition and thin-film coating in a filamentary and a glow dielectric barrier discharge. Plasma Processes Polym. 2021; e2000248. https://doi.org/10.1002/ppap.202000248

1 INTRODUCTION

Thin-film deposition by plasma-enhanced chemical vapor deposition (PECVD) on silicon wafers has first been investigated in the 60 s. Later, the PECVD technology was extended to atmospheric plasma (AP PECVD).[1–6] The main advantage of atmospheric pressure plasma is the ability to lower the costs for treating materials by avoiding pumping systems and enabling large surface treatments by a continuous process. Owing to its simple scalability from small laboratory reactors to large industrial installations and the homogeneity of deposited layer, dielectric barrier discharge (DBD)[7–9] is a good candidate for making a thin-film polymer.[10–13] For this reason, nonequilibrium atmospheric pressure plasma in a DBD configuration is an interesting option for treatment and coating of surfaces.

As reported by Massines et al.,[14] five different discharge regimes are possible while working with dielectric barrier discharges at atmospheric pressure. These regimes are filamentary DBD (FDBD), glow-like DBD (GLDBD), glow DBD (GDBD), Townsend DBD (TDBD), and radiofrequency DBD. This study will focus on two of them, selected for their differences in electron energy levels and electron density. On the one hand, FDBD is characterized by a multitude of microdischarges with a high electron density (10^{13}–10^{14} cm^{-3}) for a very short discharge duration (100 ns). On the other hand, GDBD is characterized by a homogenous discharge with a lower electron density (10^{10} to 10^{11} cm^{-3}) but a longer discharge duration (μs).[14] Previous works have shown that in identical atmospheres, FDBD and GDBD could lead to different surface treatments.[15,16] Accordingly, the

aim of this study is to better understand the differences of the chemistry occurring in the two aforementioned DBD modes. These two discharge regimes are easily obtained in Ar–NH_3 Penning gas mixture. GDBD is observed for higher frequencies. The higher repetition rate maintained a higher energy in the gas gap and induced a higher power.[14]

Ethyl lactate (EL) was chosen as a vaporized liquid precursor. This choice was motivated by two reasons. First, EL displays a wide variety of chemical bonds with various dissociation energies. These different bonds are easily detected by infrared absorption spectroscopy, allowing an in situ observation of the molecule transformation. Second, the plasma polymerization process of EL is likely to produce a "polylactic acid-like" polymer. Polylactic acid presents a great interest related to its biodegradability by water or microorganism [17,18] and its nontoxicity. It could be used for controlled drug release for biomedical application.[19–21] For this reason, scientists started to pay close attention to the synthesis of "polylactic acid-like" films through plasma-based technologies. EL plasma polymer (EL PP)[13,22,23] was shown to be biodegradable,[24] therefore paving the way for its use as a drug delivery system.

The decomposition scheme of EL has been studied using several characterization techniques, including mass spectrometry,[12,25] X-ray photoelectron spectroscopy,[10] and electrical characterizations.[6] In this study, Fourier-transform infrared (FTIR) absorption spectroscopy was used. This method is convenient to characterize both the plasma and the thin film. Space- resolved measurements were used to analyze the decomposition of EL in the plasma and the thin-film composition as a function of the gas residence time in the plasma.[26] On the one hand, the decomposition kinetics of EL in both FDBD and GDBD plasma regimes was ascertained through in situ FTIR measurements. On the other hand, the thin-film composition was also characterized by FTIR along its whole length and correlated with the EL decomposition scheme along the plasma.

2 MATERIALS AND METHODS

2.1 Materials

The experimental setup was composed of an airlock chamber in which the plasma reactor was placed. The chamber was pumped down to 2.2×10^{-2} Torr and then filled with nitrogen (Alphagaz 1, 99.999% purity) to avoid arcs formation around the electrodes. Then the vaporized liquid precursor was injected between the electrodes, together with the carrier gases. The organic precursor chosen for the study was (-)-ethyl L-lactate $C_5H_{10}O_3$ (Sigma-Aldrich) with confirmed purity at 97.5%. The carrier gas was argon (Alphagaz 1, 99.999% purity) as the main gas and NH_3 (Alphagaz 1, 99.999% purity) for ensuring discharge stability. The reactor chamber was filled with nitrogen (Alphagaz 1, 99.999% purity) for ensuring discharge stability.

2.2 Methods

2.2.1 Plasma reactor

The plasma reactor is a plane-to-plane DBD already described elsewhere.[26,27] Briefly, it was composed of two electrodes (2×5 cm^2), one is connected to a high voltage (HV) and the other is connected to the ground. The electrodes were metallized on the rear face of the alumina plates of 69×69 mm^2 and of 1 mm in thickness (Figure 1). Two transformers (Boige et Vignal) are used for these experiments. The first one is operated at a frequency range from 1 to 10 kHz, whereas the second one enables working between 50 and 100 kHz. Both transformers made it possible to work at amplified voltages (Crest CC4000 audio amplifier) ranging between 1 and 15 kV with waveforms selected using an Agilent 33210 waveform generator. The gap between the alumina plates was kept at 2 mm. EL PP was deposited on top of a 275- μm-thick round silicon wafer with 5.08 cm in diameter.

The deposition area was the same as that of the electrodes, which was 2 × 5 cm^2. The characteristics of the two DBDs of this study are given in Table 1.

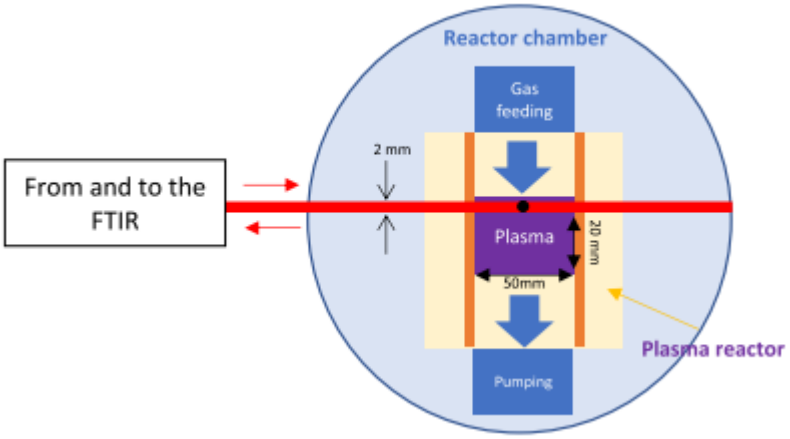

Figure 1 Experimental setup of the reactor with the Fourier- transform infrared spectroscopy (FTIR) (red line—infrared beam, yellow lines—zinc selenide windows, black dot—the position of the thin-film analysis)

Table 1 Characteristics of the chosen DBD regimes[14]

Property/Type of DBD	Filamentary DBD	Glow DBD
Frequency (kHz)	15	50
Voltage (kV)	3	1.3
Average power (W)	1	4
Average volumetric power (W/cm^3)	0.5	2
Homogeneity of the discharge	No	Yes
Maximum electron density ($1/cm^3$)	10^{13}–10^{14}	10^{10}

Abbreviations: DBD, dielectric barrier discharge; FTIR, Fourier-transform infrared spectroscopy.

The reactor chamber was pumped down to 2.2×10^{-2} Torr and then filled with nitrogen (to reach a pressure of 760 Torr). Initial filling with nitrogen minimizes arc formation around the electrodes, as nitrogen has 10 times higher breakdown voltage than argon, which has been chosen as the carrier gas due to its lower breakdown voltage, lower cost compared with helium, and its inability to incorporate itself within the molecular structure of the plasma polymer, as shown by Laurent et al.[22]

An aerosol made of 1.1 slm of argon + EL by the means of an atomizer (TSI atomizer model 3076 creating droplets in the size range between 0.3 and 3 μm) was diluted in 1.9 slm of argon + 133 ppm of NH_3, making a total flow of Ar of 3 slm containing 350 ppm of EL and 133 ppm of NH_3. This gas mixture was injected in the reactor through a 0.1×4 cm^2 slit located 4 cm away from the DBD. Two zinc selenide (ZnSe) IR transparent windows ($2 \times 2 \times 70$ mm^3) were placed parallel to the gas stream to maintain the laminar flow by avoiding any gas flow perturbations. The gas injection was perpendicular to the long axis (5 cm) of the electrode and the spectral acquisition was performed every 2 mm along the 2-cm-long plasma (Figure 2). Therefore, the position of the measurement along the plasma can be correlated with the residence time and the mean energy sensed by the species.[28,29] The voltage amplitude for each regime was chosen to ensure a stable discharge and reproducibility of the results. As the power is the integral of the product of the measured voltage and current over a cycle divided by the cycle duration, it is the result of the chosen plasma parameters.

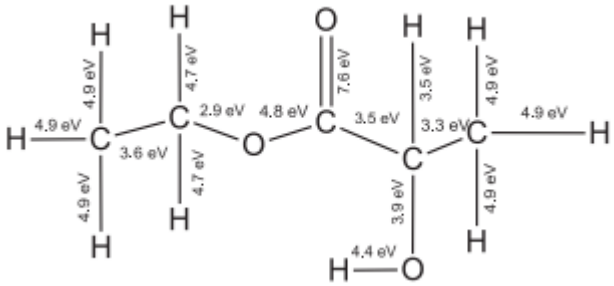

Figure 2 Structure of ethyl lactate with energies needed to dissociate its chemical bonds[30]

2.3 In-flight precursor FTIR

The FTIR setup used to record in-flight and in situ spectra of the precursor, in both gaseous and plasma phases, is described elsewhere.[26] The spectrometer was an Agilent Cary 670 equipped with a KBr beam splitter and a narrowband MCT-A detector. The spectra were recorded between 4000 and 400 cm^{-1} by co-adding 256 scans at a resolution of 4 cm^{-1}. The absorption length across the plasma was 10 cm, corresponding to a back- and-forth passage along the long axis of the electrodes.

The background spectrum was recorded in pure argon without plasma, whereas the plasma spectra were recorded 5 min after injecting EL at a concentration of 350 ppm in argon in the plasma reactor. This was done to ensure constant and reproducible amount of EL in the gas between the electrodes at the time of lighting up the discharge.

The infrared beam path located outside the reactor was always purged with dry CO_2-free air. The plasma reactor was systematically pumped down between each experiment. It is worth noting that CO_2 absorption was never observed without plasma. After each measurement with EL, the plasma region was flushed with pure argon. Another spectrum was recorded in these conditions and

subtracted from that of the EL plasma. This enabled to eliminate the spectral contribution of adsorbed EL on the ZnSe windows. However, a decrease of the peak-to-peak voltage intensity of the interferogram at the beginning and at the end of each experiment has never been observed, therefore, indicating that the effect of plasma deposition of the ZnSe windows on the FTIR signal was marginal.

The resulting spectra were then smoothed using Origin FFT filter with 5 points to improve the accuracy of the measured peak absorbances. Five analysis positions were considered for both plasma and thin-film analysis at 0 ± 1, 5 ± 1, 10 ± 1, 15 ± 1, and 19 ± 1 mm along the 2-cm-long plasma, and the corresponding mean residence time of the gases in the plasma is 1.2 ± 1.2, 6.0 ± 1.2, 12.0 ± 1.2, 18 ± 1.2, and 24 ± 1.2 ms, respectively. Calibration curves were built to follow the concentration of each of the EL chemical bonds by measuring their infrared absorbance while injecting EL between the electrodes at concentrations ranging from 0 to 700 ppm without igniting the plasma. The quantification limits, defined as being 10 times the standard deviation of noise fluctuation,[31] are reported in Table 2. As CO_2 is a decomposition product of EL,[11] it was calibrated by measuring the integrated absorbance of the 2340–2360 cm^{-1} feature of infrared spectra recorded with known amounts concentration of CO_2 introduced in the plasma chamber.

Table 2 Infrared assignments of the observed absorptions: Ethyl lactate and carbon dioxide[11,32–34] and their quantification limits in the experimental conditions of this study

	Wavenumber (cm^{-1})	Vibrational mode	Quantification limit (ppm)
P_1	3570–3200 (broad)	OH stretching (intermolecular)	150
P_2	2990	CH_3 asymmetric stretching	90
P_3	2940	CH_2 asymmetric stretching	186
P_4	1750	Ester group, C–(C=O)–R Ketone, R_1–(C=O)–R_2 asymmetric stretching	38
P_5	1620	Carboxylate group, R–(C=O)–O	
P_6	1455	CH_x bending	
P_7	1380	Primary or secondary, OCO–H (intramolecular) in-plane OH bend	158
P_8	1266	$CH(OH)CH_3$ bending	158
P_9	1222	C–OC(=O) stretch	
P_{10}	1140	C-OH asymmetric stretching	44
P_{11}	2360–2340	C=O in CO_2	5
P_{12}	3575	Free OH	

2.4 Thin-film FTIR

A Nicolet 6700 (Thermo Fisher Scientific) FTIR spectrometer purged with CO_2-free dry air was used to analyze the thin films. The thin-film transmission spectra were the results of the co-addition of 64 scans at a resolution of 4 cm^{-1}. The spectrum of a clean silicon wafer was first recorded and subtracted from the spectrum of the plasma-polymerized EL on silicon. Measurements were made with a 2-mm spatial resolution along the direction of the gas flow (i.e., 2 cm) and were made in the middle of the 5-cm-wide plasma-deposited coating (black point in Figure 1), to compare spectra recorded at the corresponding positions in the plasma and on the thin film. The degree of polymerization of the plasma- deposited film was evaluated by calculating the P_3/P_2 ratio (see Table 2 for peak assignments). First, a second-order polynomial function was used for baseline correction between 2700 and 3250 cm^{-1}, therefore enabling to eliminate the spectral contribution arising from the OH stretching mode. The aforementioned P_3/P_2 value was then calculated by ratioing the absorbance of the shoulder at 2940 cm^{-1} on that of the peak maximum at 2990 cm^{-1}.

3 RESULTS AND DISCUSSION

The use and importance of EL in this study was attributed to its efficient absorption in infrared, useful for its characterization by FTIR, its biocompatibility, and nontoxicity. It also has well-defined and distinctive energies for dissociating a given bond within the molecule (Figure 2), which also makes it an interesting candidate to determine the plasma chemical reactivity.

3.1 FTIR spectra

Figure 3 presents normalized spectra (to the peak at 1750 cm^{-1}) of EL in-gas phase with and without plasma and of the "polylactic acid-like" polymer coating. All three spectra show the usual IR absorption of EL, as listed in Table 2. However, differences are observed. The peaks in EL in the gas phase are easily distinguishable, compared with the solid phase, where overlapping between absorption bands can be observed. This is due to the lesser number of interactions between molecules in the gas phase as compared with the thin film. In addition, the plasma spectrum shows significantly higher noise-to-signal ratio as compared to the gas phase without plasma, due to the electromagnetic noise. The first striking observation is the almost complete disappearance of the OH stretching mode feature (P_1) in both the gas and plasma made with EL due to the absence of intramolecular interactions in these phases. In addition, the absorbance of P_{12} (free OH stretching) decreases from the gas phase to the plasma, with a concomitant appearance of P_1 in the deposited thin-film spectrum. Another observation that is worth mentioning is the creation of CO_2, manifested through the feature at 2340–2360 cm^{-1} (P_{11}), without any gaseous H_2O production, only observed in the plasma.

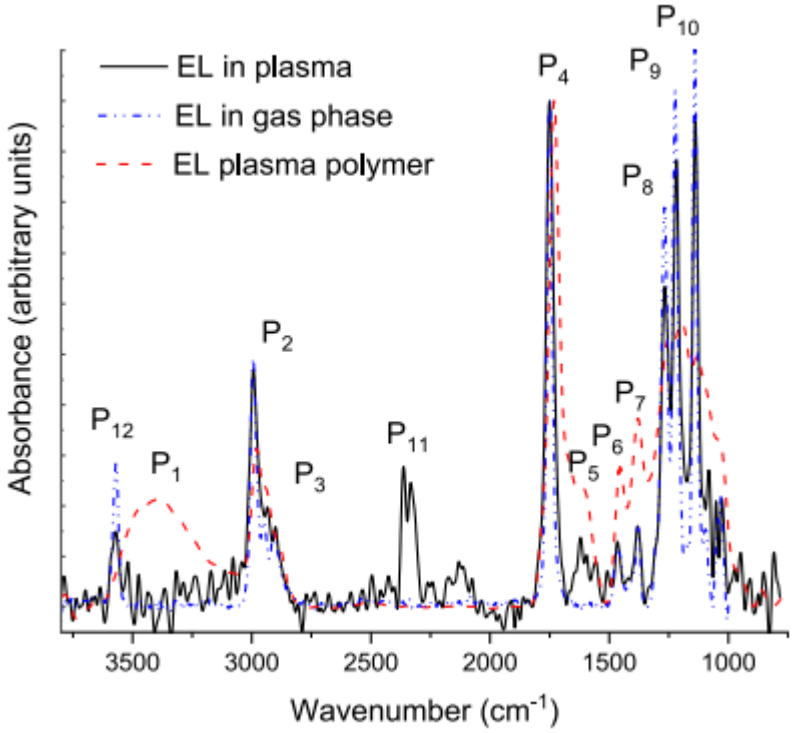

Figure 3 Typical normalized Fourier-transform infrared spectra of ethyl lactate (EL) in the gas with (solid black line) and without (blue dash-dotted line) plasma, and of the "polylactic acid- like" polymer thin film (red dashed line) state

3.2 In situ plasma FTIR analysis

3.2.1 Glow DBD

Figure 4 presents the plasma IR absorptions at 5 different positions in a GDBD along the gas flow, for example, for 5 different gas residence times in the plasma. Peak identification reported in the graphs corresponds to those of Table 2. The overall tendency is that the EL absorption bands decrease when this precursor residence time in the gas increases, showing a continuous fragmentation of the molecule along the plasma. At the same time, the concentration of CO_2 (P_{11}) increases along the plasma. As no H_2O absorption is observed, the CO_2 formation cannot be explained by combustion reactions, meaning that the discharge does not entirely decompose the molecule (as in combustion process, for instance) but mostly fragments EL.

From Figure 4, it can be seen that the so-called decrease of the P_{12} absorbance begins between positions 5 and 10 mm in the plasma, therefore showing that dissociation of this chemical group from the overall EL molecule starts somewhere from these positions.

It is also interesting to observe the behavior of the CH_2 and CH_3 groups of the EL molecule in the plasma, which can be followed through either their stretching (P_2 and P_3) or bending (P_6) modes. As may be seen in Figure 4, CH_x stretching mode features (P_2 and P_3) remain present for all plasma positions, whereas CH2 and CH_3 bending (P_6) is much less intense. This is a clear indication that some of the CH_2 and CH_3 groups of EL lose some of their hydrogen atoms to form CH containing moieties, which still can give rise to C–H stretching mode spectral contributions but, of course,

cannot provide bending vibrations, as at least two hydrogen atoms need to be bound to a single carbon for such spectral contributions to be observed. Finally, the absorbance of the C=O (P4), C–OC (P_9), and C–OH (P_{10}) stretching mode features also tends to decrease along the plasma, whereas their wavenumbers remain in the range typical of esters (P_9) and/or aldehyde (P_{10}), showing that these bonds are still present in the plasma phase.

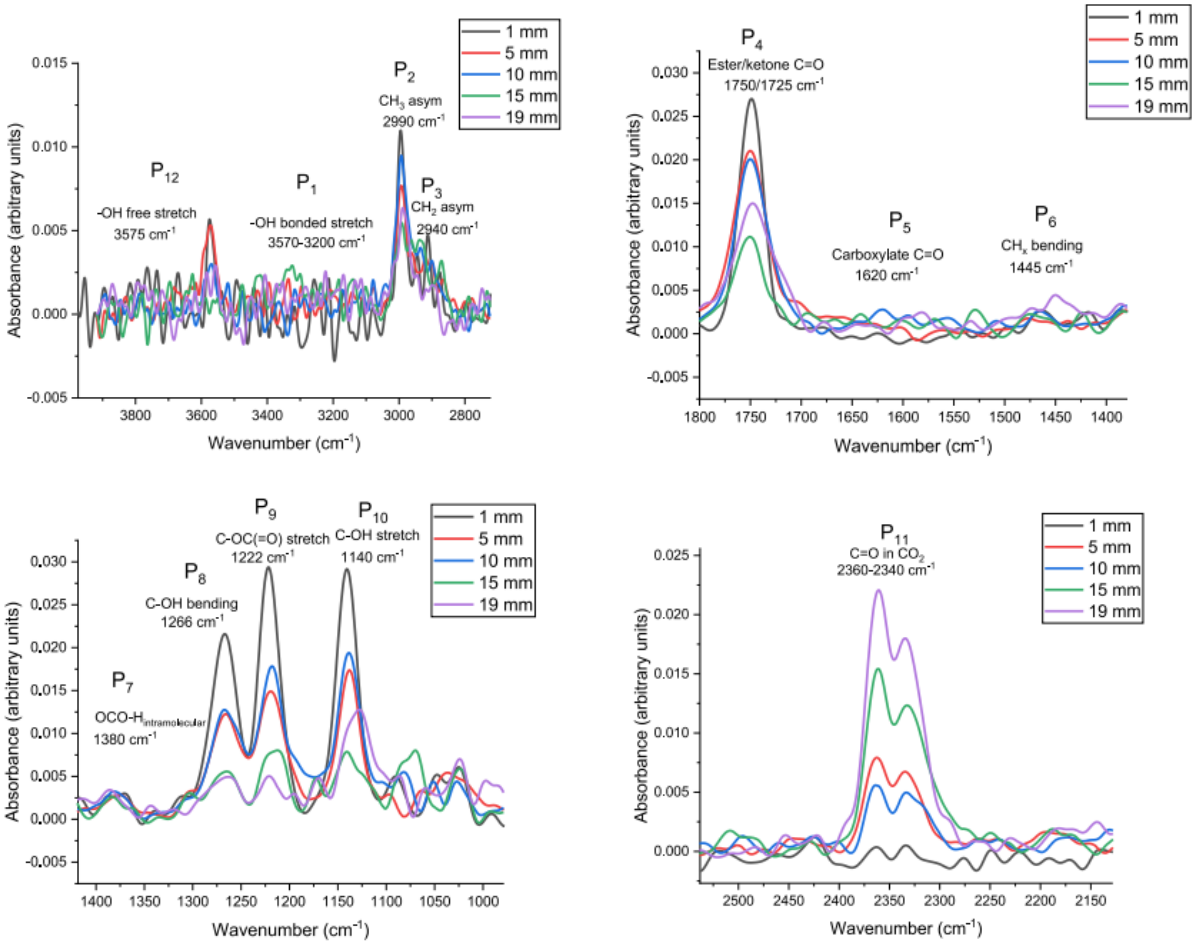

Figure 4 Ethyl lactate (EL) bands by position in glow dielectric barrier discharge regime from the plasma phase spectra. Higher is the position, the longer is the EL residence time in the plasma

3.2.2 Comparison of glow and filamentary DBD

Figure 5 shows the comparison of the concentration evolution of some selected chemical groups with the energy provided per EL molecule injected in the plasma for both GDBD and FDBD. Energy is the product of the gas residence time and the DBD power. This energy could potentially be transferred to the EL molecule and to the plasma-dissociated EL molecule fragments. As the GDBD power is four times larger than that of the FDBD (Table 1) with identical EL concentration, the energy per EL molecule is also four times larger in the GDBD. The conversion from absorbance to concentration was made based on the aforementioned calibration curves (see Section 2). The selected chemical groups are related to C–O, C–H, and O–H bonds of EL and CO_2 molecules. The

error bars are obtained by calculating the error propagation from intensity to concentration, from the standard deviation of the intensity measurements and the uncertainty of the calibration curves.

Generally speaking, the various chemical species concentration evolution with the energy provided per EL molecule follows a similar trend for both GDBD and FDBD. However, GDBD leads to a more gradual decomposition of EL, whereas FDBD shows rather large oscillations. Indeed, FTIR measurements last about a minute, whereas the repetition rate of the FDBD is 15 kHz (0.067 ms). Accordingly, FTIR measurements lead to concentration values that are averaged in time. In addition, the IR absorption path length is much longer (10 cm) than the microdischarge radius (typically 200 µm)[14] with a mean distance between two microdischarges in the range of mm. These two observations point toward the fact that the various chemical group observed concentration oscillations are real, which is confirmed by the reproducibility of the measurements. However, the origin of these oscillations is still unclear at the present time. Interestingly, the CH_3 and CH_2 (P_2 and P_3) concentrations sometimes reach higher values than what would have been expected from the single injection of EL, indicating that another source is responsible for these moieties production. As a very high concentration of energetic species is reached locally and for a short time in an FDBD as compared with GDBD, in which energetic species concentrations are lower and more uniformly distributed, it is theorized that surface etching occurs in FDBD, as already observed by Jidenko et al.,[35] therefore leading to this increase of hydrocarbon moieties in the plasma discharge.

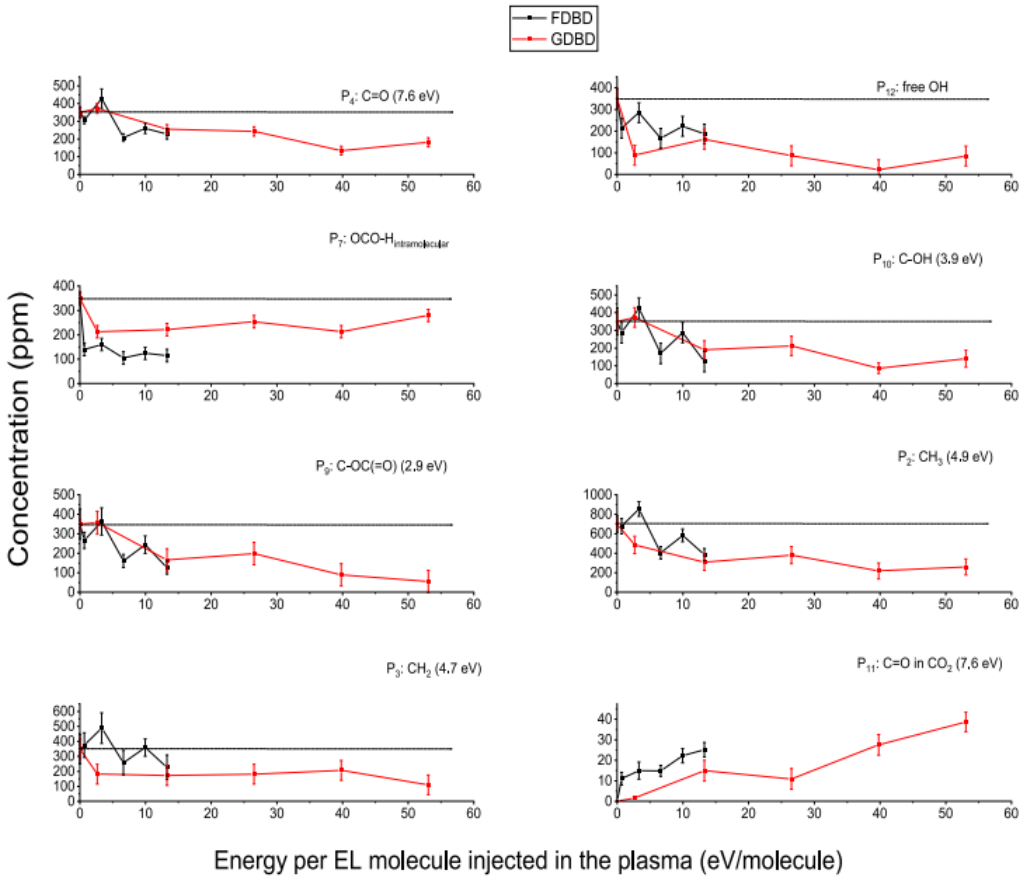

Figure 5 Evolution of concentration of different infrared absorption bands in both glow dielectric barrier discharge (GDBD) (red) and filamentary dielectric barrier discharge (FDBD) (black) as a function of energy per ethyl lactate (EL) molecule in the plasma phase. The values at 0 eV were taken from vaporized EL without plasma (black dashed line represents that initial concentration without plasma)

For FDBD, the C═O (P_4) chemical bond behavior shows that the concentration in the plasma oscillates in the first two positions and then stabilizes at around 225 ppm at 10 eV/molecule and does not change significantly as more energy per molecule is provided. In this plasma regime, both C–OH (P_{10}) and C–OC (P_9) follow this similar oscillating trend between positions, but in general show a decrease from the beginning to the end of the plasma zone and reach a minimum of around 125 ppm. When 3 eV/molecule is provided, both CH_3 (P_2) and CH_2 (P_3) show a greater concentration, owing to the initially injected EL, probably due to the fact that the FDBD could induce etching of the surface and reintroduction of fragments into the plasma region. With the increase of the energy provided to each EL molecule, the concentrations of these hydrocarbon moieties decrease to reach 450 and 250 ppm, respectively. However, the concentration of free OH (P_{12}) in the FDBD decreases by position to reach 200 ppm for 15 eV/molecule. Interestingly, the amount of OCO–H_{intra} (P_7) decreases significantly as EL enters the plasma and then reaches a plateau of around 100 ppm at 6 eV/molecule, which does not change with more energy being provided to each molecule.

As mentioned previously, the concentration changes in GDBD are distinctive of those in FDBD. In GDBD C═O (P_4), C–OH (P_{10}), and CH_3 (P_2) show a similar behavior with the increasing energy, where a slight decrease is observed until 40 eV/molecule is reached and then plateaus at 200, 150, and 300 ppm, respectively. The concentration of C–OC (P_9) bonds decreases steadily with the increasing energy and reaches a concentration very close to 0 ppm, coherent with the fact that this is the bond with the lower dissociation energy in the EL molecule. A decrease is observed at 4 eV/molecule for CH_2 (P_3) concentration, which plateaus at 175 ppm between 2.5 and 40 eV/molecule and then decreases to 100 ppm at 52 eV/ molecule. The free OH group concentration (P_{12}) shows a rather continuous decrease up to 40 eV/molecule where it reaches a concentration close to 0 ppm. A slight increase is observed at the very exit of the plasma discharge area, suggesting creation of free OH likely due to the important fragmentation of the whole molecule at these energy levels. Similar to what was observed with FDBD, the concentration of OCO–H_{intra} (P_7) in the GDBD decreases from 350 to 210 ppm at 4 eV/molecule and then plateaus up to 40 eV/molecule to finally slightly increase to reach final concentration of 300 ppm.

3.2.3 Carbon dioxide creation from EL dissociation in the plasma phase

One of the important byproducts of plasma dissociation of EL is CO_2, which necessarily comes from the dissociation of either C–OC, C–OH, or C═O moieties. Thus, the concentration of CO_2 was plotted as a function of the consumption of these oxygen-containing functionalities. Among the plotted curves, only the consumption behavior of C–OC (P_9) in GDBD regime was shown to follow trend that could be reasonably defined by a mathematical equation. The results are presented in Figure 6.

As it is seen in Figure 6, in GDBD regime, the creation of CO_2 as a function of C–OC consumption follows a quadratic relationship, which reaches a maximum of 40 ppm of carbon dioxide. In terms of decomposition mechanism, such a quadratic relationship means that two C–OC moieties are involved in the formation of a single carbon dioxide molecule. A similar quadratic relationship was also observed in GDBD for the production of CO_2 as a function of C–OH groups (not shown). However, no clear relationships were found between CO_2 production and C═O moieties consumption in the GDBD regime and any of the EL oxygen-containing moieties in FDBD conditions. The origin of these differences in terms of CO_2 production between these two plasma regimes still has to be elucidated.

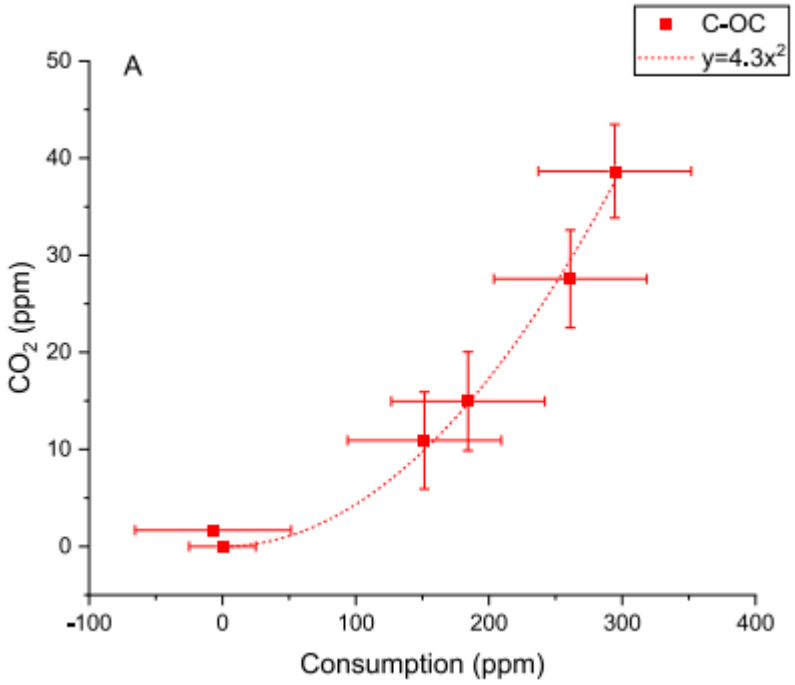

Figure 6 CO_2 concentration as a function of the decomposition of A: C–OC (P_9) for glow dielectric barrier discharge

3.3 Thin-film spectra

3.3.1 Comparison between plasma- and solid-phase spectra

Figure 7 compares the plasma and thin-film FTIR spectra at the same position in the plasma discharge. At first sight, it has to be emphasized that all of the features observed in the infrared spectrum of the plasma phase are seen in that of the solid film, which means that all of the chemical functionalities of the EL molecule are, at least, partly transferred in the chemical structure of the plasma-polymerized film. For those infrared bands occurring in both the plasma and the solid phases, the general trend is that infrared peaks of the film are shifted to lower wavenumbers, in agreement with a higher level of order with respect to the plasma phase.[32,36] In addition, the infrared features of the thin-film spectrum are also broader, in agreement with the fact that more molecular interactions occur in the solid as opposed to the plasma phase.[32]

Some spectral regions are of particular interest while comparing the chemical composition of both plasma and solid phases. First, the OH stretching mode vibration (P_{12}) does not appear in the spectrum of the plasma, but a rather narrow band with a low absorbance appears at 3575 cm^{-1} and is assigned to free OH stretching vibrations (P_{11}), as few molecular interactions are likely to occur in the plasma phase. However, in the plasma polymer spectrum, the presence of the OH groups is rather observed through a much wider feature centered around 3400 cm^{-1} (P_1), which reflects the fact that these chemical moieties are involved in several interactions such as hydrogen bonds.

Major differences are also observed while comparing the C═O (P_4) stretching mode vibration region of both the plasma and solid phases. As seen in Figure 7, the infrared spectrum of the plasma phase exhibits an absorption at 1750 cm^{-1}, assigned to the ester function of EL. In the spectrum of the polymer film, this band is shifted to 1725 cm^{-1}. In addition to the aforementioned ordering effect observed when EL is converted from the plasma to the solid phase, the specific wavenumber value

of this infrared component may also be due to the fact that the ester group of the EL molecule is converted into a ketone. This presence of a ketone in the thin film could mean that the preferential group to be dissociated is the C–OC (P_9) group, which is the lowest energy bound of EL.

It is worth noting that another C═O (P_5) stretching mode feature appears near 1600 cm^{-1} in the infrared spectrum of the plasma polymer film, which is generally assigned to the presence of carboxylate groups. All in all, this means that the EL ester groups are, at least partly, converted into ketones and carboxylic acid functionalities. The OH components of these latter chemical groups are also likely to contribute to the so-called C–OH stretching mode (P_{10}) feature observed in the infrared spectrum of the plasma-deposited film.

Finally, comparison between the C–OC (P_9) and C–OH (P_{10}) stretching mode features (P_9 and P_{10}) for both the plasma and solid phases clearly puts in evidence the aforesaid ordering effect along with the increase of the number/intensity of the molecular interactions, as seen through these peaks broadening and shift to lower wavenumbers.

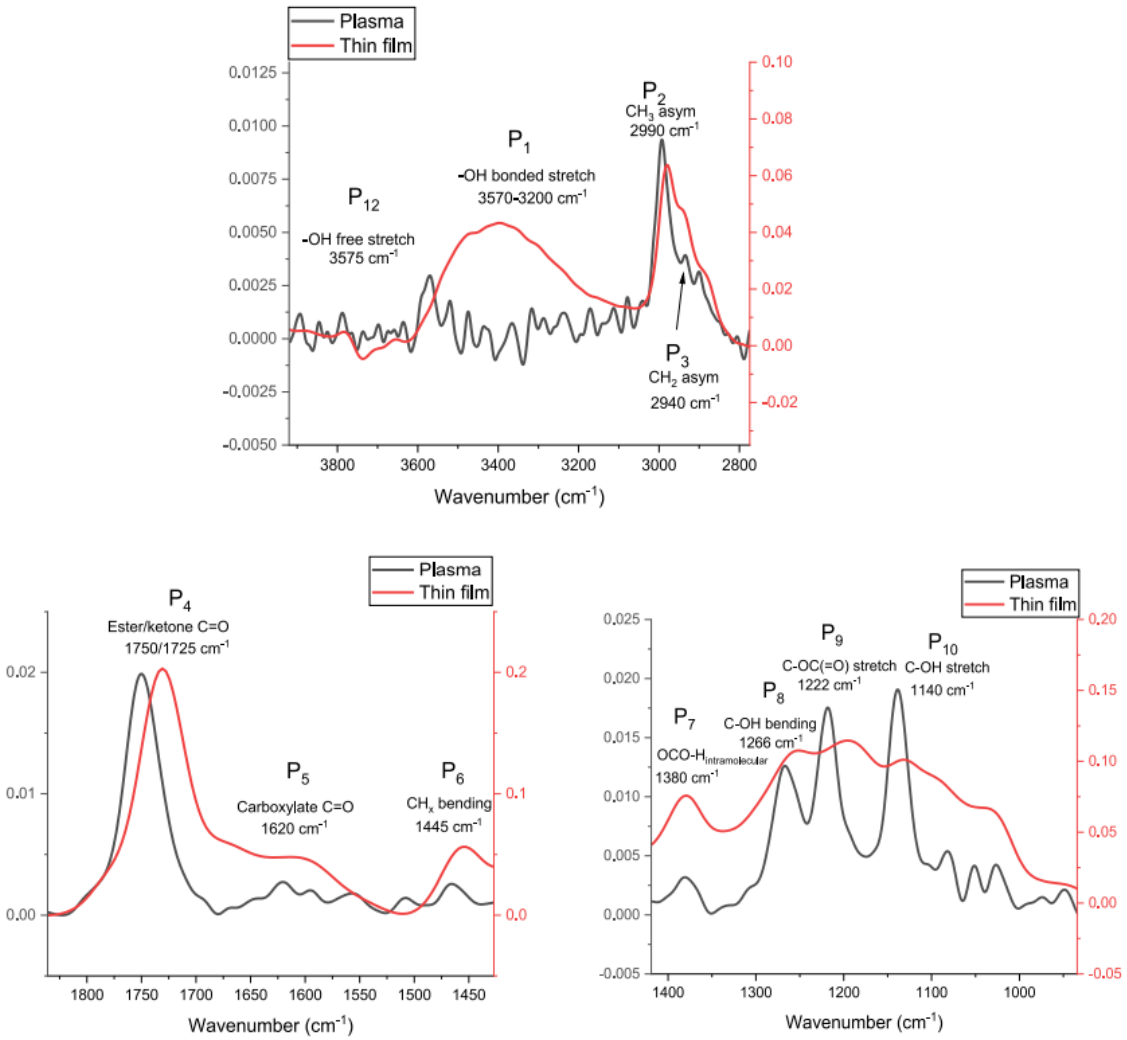

Figure 7 Comparison of ethyl lactate band evolution in both plasma phase (black) and plasma polymer (red) at 10 mm for glow dielectric barrier discharge regime

3.3.2 Thin-film polymerization level

To try to probe the level of EL polymerization along the plasma, the infrared CH_2/CH_3 ratio (P_3/P_2) was measured for each investigated position across the plasma- deposited film. The idea of using this ratio to monitor the EL polymerization level is based on the fact that methyl groups (CH_3, P_2) are likely to be mostly found at the end of polymeric chains. Accordingly, it is expected that long EL polymeric chains would be characterized by a high CH_2/CH_3 infrared ratio, with, of course, no polymerization occurring when this spectroscopic parameter is equal to that of pure EL.[37,38]

According to the defined criteria, Figure 8 shows that the plasma-polymerized film deposited under the FDBD regime is more polymerized than the GDBD for all investigated positions, and GDBD shows a greater uniformity in the polymerization throughout all the positions of the coating.

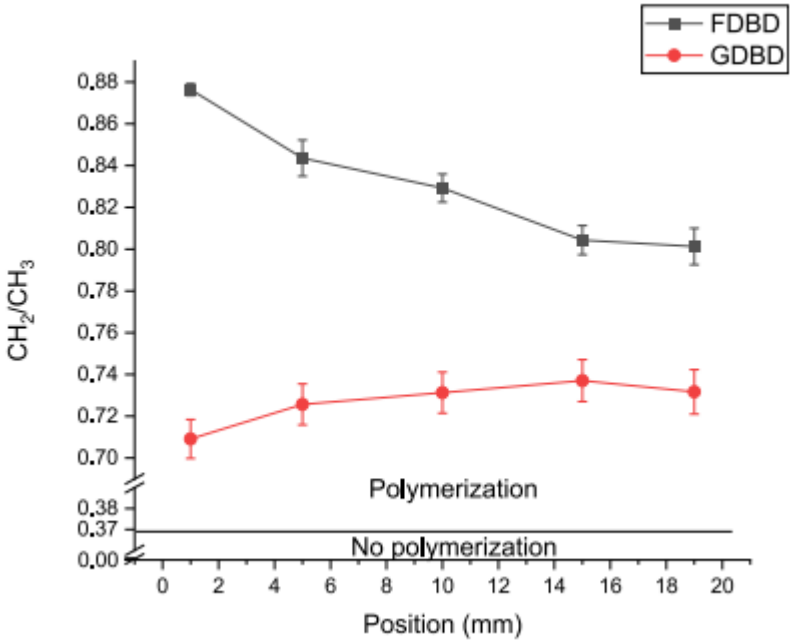

Figure 8 CH_2/CH_3 infrared ratio measured from the spectra of plasma-polymerized films at positions corresponding to each investigated location in the plasma for filamentary dielectric barrier discharge (FDBD) (black) and glow dielectric barrier discharge (GDBD) (red). The horizontal line indicates the CH_2/CH_3 ratio for pure gaseous ethyl lactate (EL) (no polymerization)

3.4 Thin-film coating and the DBD chemistry

To try to follow the incorporation of the various EL chemical groups within the plasma-deposited films, the absorbance of some of the infrared features of these coatings were ratioed to the absorbance of the C═O stretching mode peak (P_4). The absorbance of this latter feature was fairly constant throughout the length of the plasma-deposited film (results not shown). These ratios were, in turn, divided by their corresponding counterparts measured from the infrared spectrum of liquid EL. In other words, these calculations (A_N) enable comparing the thin-film and liquid EL composition, in terms of their respective relative amount of a given chemical group and the carbonyl functionality, and are described by the following mathematical equation:

$$A_N = \frac{A_{BTF}/A_{C=OTF}}{A_{BL}/A_{C=OL}},$$

where A_{BTF} is the absorbance of the infrared features of interest in the plasma-deposited thin films, $A_{C=OTF}$ is the absorbance of the C=O stretching mode band in the thin film, A_{BL} is the absorbance of the so-called peaks of interest in liquid EL, and $A_{C=OL}$ is the absorption of C=O in the liquid EL. Accordingly, an A_N value lower than 1 means that the relative amount of a given chemical group, as compared with the carbonyl functionalities, is lower in the film than in the EL molecule, whereas an A_N value higher than one signifies that the plasma- polymerized film contains relatively more of the chemical functionality of interest with respect to what is observed in the EL molecule.

Figure 9 shows the results of these calculations made by correlating the information originating from infrared spectra recorded at identical positions in the plasma phase and deposited thin films for both FDBD and GDBD regimes.

Very interesting observations can be drawn from this figure. From a general standpoint, and regardless of the plasma regime, the amount of a given chemical species in the plasma-polymerized film does not depend on this chemical functionality concentration within the plasma, as all relationships between A_N and the in-plasma species concentrations can be fairly well described by a horizontal line. For example, A_N measured from the C–OC spectral contribution (P_9) only slightly varies around a value of 0.5 with, however, a rather large variation of the concentration of this chemical functionality in the plasma, which spans from approximately 100 to 350 ppm. It is worth noting that the in-plasma concentration of the OCO–H_{intra} group (P_7) is almost identical (approx. 100 ppm) for both plasma regimes and positions. Second, and also regardless of the plasma regime, the relative amount of oxygen-containing species is clearly lower in the plasma-polymerized film than in the EL precursor molecule. This is in agreement with the data presented in Figure 6, which show that some of the EL oxygen-containing species are converted in CO_2, therefore not being available anymore to be incorporated in the plasma polymer film. Third, the hydrocarbon moieties are the only ones that are observed in greater relative amount in the plasma coating as compared with the EL molecule. For these latter moieties, the plasma regime clearly has an influence as relatively more CH_2 and CH_3 groups are incorporated in the plasma coating with respect to the EL molecule in the FDBD regime, whereas an opposite behavior is observed in the GDBD mode. In the FDBD regime, the A_N values calculated for CH_2 groups are all higher than the corresponding data for CH_3 functionalities, in agreement with the results presented in Figure 8, which shows more precursor polymerization in the filamentary mode. It is also interesting to highlight the fact that the preservation of a given chemical functionality from the precursor to the plasma coating is not necessarily related to the bonding energy. For instance, the C–OC (2.9 eV) chemical groups are more "preserved" in the plasma polymer structure than the CO–H (3.9 eV) functionalities. This emphasizes the fact that the inherent reactivity of chemical groups should also be taken into account to explain the decomposition mechanisms of organic precursors within plasma.

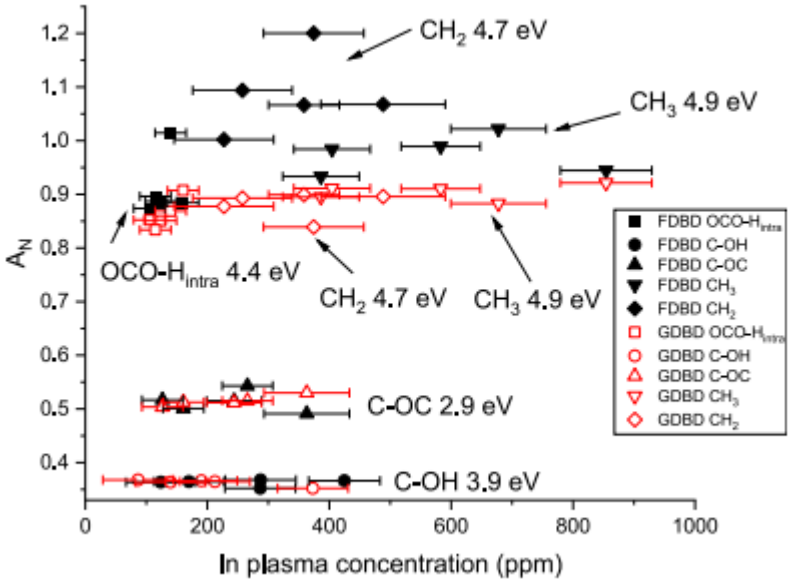

Figure 9 Normalized thin-film absorbance of different bonds as a function of the filamentary dielectric barrier (FDBD) discharge and glow dielectric barrier discharge (GDBD) plasmas concentration by the same bond

4 CONCLUSIONS

This study has compared EL decomposition in the plasma and thin-film deposition using atmospheric pressure Ar DBD in both filamentary and glow regimes. The power of the GDBD is four times than that of the FBDB. Measurements were made as a function of the position along the gas flow, for example, EL residence time in the plasma, which is directly correlated with the energy provided per EL molecule.

The analysis consisted of a thorough space-resolved study and comparison of the FTIR spectra in the plasma phase and of the thin films. Given the plethora of absorption bands present in the EL infrared spectrum, the most characteristic features with known assignments have been selected for analysis of the two phases.

In the FDBD regime, the analyses suggest that etching could be occurring from the already deposited layer, which results in oscillations of the concentration of the chosen absorption bands in the IR spectra of the plasma phase. Moreover, in certain cases, the amount of the observed fragment is greater in the plasma phase than that of the injected precursor, reaffirming the etching hypothesis. For the GDBD regime, the decomposition of EL is much more gradual throughout the plasma width and generally results in a greater decomposition than that of FDBD when the same time of residence is taken into account.

As a result of bond dissociation, CO_2 creation is observed in both regimes. In GDBD, there is a quadratic relationship between the production of CO_2 and the consumption of C–OC groups. In FDBD, CO_2 formation requires less energy than in GDBD, perhaps related to the high electron density of the microdischarges, resulting in CO_2 saturation early in the plasma zone. However, the FDBD regime does not show a correlation between decomposition of oxygen-containing species and CO_2 creation. GDBD allows to reach 40 ppm of CO_2 as compared with 25 ppm in FDBD.

Moreover, the CH_2/CH_3 peak height intensity ratio measured from the infrared spectra of plasma-deposited films demonstrates that the polymerization level is higher when using the FDBD regime as opposed to the GDBD mode, but the polymerization in the coating created with GDBD is more homogenous throughout the coating.

The analysis of the deposited layer as a function of the decomposition of the molecule in the plasma phase showed that there is a dependence of the bond dissociation energy and the preservation of a fragment in the plasma polymer, as the bonds with highest energies are deposited in a greater amount in the coating and the opposite is seen for the low energy bonds. Another noteworthy observation was that not only the bond dissociation energy, but also the fragments reactivity plays a role in the decomposition mechanisms and the amounts of that fragment being deposited on the substrate, as seen for C–OH, which despite the higher dissociation energy than C–OC, is less preserved on the coating.

ACKNOWLEDGEMENTS

The authors would also like to acknowledge the work of Jean-Paul Hoang Hoa Dung for help with obtaining the data for the calibration curves. This study was supported by French "Investments for the future" ("Investissements d'Avenir") program managed by the National Agency for Research (ANR) under contract ANR-10-LABX-22-01 (labex SOLSTICE). The financial support of the Natural Science and Engineering Research Council (NSERC) of Canada is also acknowledged. N. Milaniak is the recipient of a scholarship from the Fondation du Centre de Recherche du CHU de Québec-Université Laval.

CONFLICT OF INTERESTS

The authors declare that there are no conflict of interests.

ORCID

Natalia Milaniak http://orcid.org/0000-0002- 0758-0955
Gaétan Laroche https://orcid.org/0000-0003-0661-628X
Françoise Massines https://orcid.org/0000-0002-9985-342X

REFERENCES

(1) S. E. Alexandrov, N. McSporran, M. L. Hitchman, Chem. Vap. Deposition 2005, 11, 481. https://doi.org/10.1002/cvde.200506385

(2) V. Hopfe, D. Rogler, G. Maeder, I. Dani, K. Landes, E. Theophile, M. Dzulko, C. Rohrer, C. Reichhold, Chem. Vap. Deposition 2005, 11, 510. https://doi.org/10.1002/cvde. 200406343

(3) V. Hopfe, R. Spitzl, I. Dani, G. Maeder, L. Roch, D. Rogler, B. Leupolt, B. Schoeneich, Chem. Vap. Deposition 2005, 11, 497. https://doi.org/10.1002/cvde.200406352

(4) S. Kang, R. Mauchauffé, Y. S. You, S. Y. Moon, Sci. Rep. 2018, 8 16684. https://doi.org/10.1038/s41598-018-35154-4

(5) S. E. Alexandrov, M. L. Hitchman, Chem. Vap. Deposition 2005, 11, 457. https://doi.org/10.1002/cvde.200500026

(6) R. Bazinette, R. Subileau, J. Paillol, F. Massines, Plasma Sources Sci. Technol. 2014, 23, 035008. https://doi.org/10. 1088/0963-0252/23/3/035008

(7) A. Al-Abduly, P. Christensen, Plasma Sources Sci. Technol. 2015, 24, 065006. https://doi.org/10.1088/0963-0252/24/6/065006

(8) M. F. Mustafa, X. Fu, Y. Liu, Y. Abbas, H. Wang, W. Lu, J. Hazard. Mater. 2018, 347, 317. https://doi.org/10.1016/j. jhazmat.2018.01.021

(9) B. Lee, D.-W. Kim, D.-W. Park, Plasma Chem. Plasma Process. 2019, 40, 61. https://doi.org/10.1007/s11090-019-10024-7
(10) S. Ligot, F. Renaux, L. Denis, D. Cossement, N. Nuns, P. Dubois, R. Snyders, Plasma Processes Polym. 2013, 10, 999. https://doi.org/10.1002/ppap.201300025
(11) S. Ligot, M. Guillaume, P. Raynaud, D. Thiry, V. Lemaur, T. Silva, N. Britun, J. Cornil, P. Dubois, R. Snyders, Plasma Processes Polym. 2015, 12, 405. https://doi.org/10.1002/ppap.201400123
(12) S. Ligot, M. Guillaume, P. Gerbaux, D. Thiry, F. Renaux, J. Cornil, P. Dubois, R. Snyders, J. Phys. Chem. B 2014, 118, 4201. https://doi.org/10.1021/jp411244x
(13) S. Watson, B. Nisol, S. Lerouge, M. R. Wertheimer, Langmuir 2015, 31, 10125. https://doi.org/10.1021/acs.langmuir. 5b02794
(14) F. Massines, C. Sarra-Bournet, F. Fanelli, N. Naudé, N. Gherardi, Plasma Processes Polym. 2012, 9, 1041. https://doi.org/10.1002/ppap.201200029
(15) F. Massines, R. Messaoudi, C. Mayoux, Plasmas Polym 1998, 3, 43.
(16) C. Sarra-Bournet, S. Turgeon, D. Mantovani, G. Laroche, Plasma Processes Polym. 2006, 3, 506. https://doi.org/10.1002/ppap.200600012
(17) R. Auras, B. Harte, S. Selke, Macromol. Biosci. 2004, 4, 835. https://doi.org/10.1002/mabi.200400043
(18) L. S. Nair, C. T. Laurencin, Prog. Polym. Sci. 2007, 32, 762. https://doi.org/10.1016/j.progpolymsci.2007.05.017
(19) K. S. Chu, A. N. Schorzman, M. C. Finniss, C. J. Bowerman, L. Peng, J. C. Luft, A. J. Madden, A. Z. Wang, W. C. Zamboni, J. M. DeSimone, Biomaterials 2013, 34, 8424. https://doi.org/10.1016/j.biomaterials.2013.07.038
(20) D. Pandita, S. Kumar, V. Lather, Drug Discov. Today 2015, 20, 95. https://doi.org/10.1016/j.drudis.2014.09.018
(21) N. Milaniak, G. Laroche, F. Massines, Plasma Processes Polym. 2020, 121, 800. https://doi.org/10.1002/ppap.202000153
(22) M. Laurent, J. Koehler, G. Sabbatier, C. A. Hoesli, N. Gherardi, G. Laroche, Plasma Processes Polym. 2016, 13, 711. https://doi.org/10.1002/ppap.201500211
(23) B. Nisol, S. Watson, S. Lerouge, M. R. Wertheimer, Plasma Processes Polym. 2016, 13, 965. https://doi.org/10.1002/ppap. 201600099
(24) C. S. M. Pereira, V. M. T. M. Silva, A. E. Rodrigues, Green Chem. 2011, 13, 2658. https://doi.org/10.1039/c1gc15523g
(25) Y. Takahashi, T. Higuchi, O. Sekiguchi, M. Hoshino, S. Tajima, Int. J. Mass Spectrom. 1998, 181, 89. https://doi.org/10.1016/S1387-3806(98)14178-7
(26) G. Laroche, J. Vallade, R. Bazinette, P. van Nijnatten, E. Hernandez, G. Hernandez, F. Massines, Rev. Sci. Instrum. 2012, 83, 103508. https://doi.org/10.1063/1.4761925
(27) P. Brunet, R. Rincón, J.-M. Martinez, Z. Matouk, F. Fanelli, M. Chaker, F. Massines, Plasma Processes Polym. 2017, 14, 1700041. https://doi.org/10.1002/ppap.201700049
(28) H.-H. Doh, Y. Horiike, J. Appl. Phys. 2001, 40, 3419. https://doi.org/10.1143/JJAP.40.3419
(29) N. Milaniak, P. Audet, P. R. Griffiths, F. Massines, G. Laroche, J. Phys. D: Appl. Phys. 2020, 53, 53. https://doi.org/10.1088/1361-6463/ab4777
(30) T. L. Cottrell, The Strengths of Chemical Bonds, 2nd ed., Butterworths Scientific Publications, London, UK 1958. https://books.google.ca/books?id=HKg6AAAAMAAJ&redir_esc=y.
(31) D. MacDougall, W. B. Crummett, et al, Anal. Chem., 2242.
(32) J. Coates Encyclopedia of Analytical Chemistry: Applications, Theory and Instrumentation (Ed.: R. A. Meyers), John Wiley & Sons, Toronto 2006.
(33) Y.-C. Ning, Interpretation of Organic Spectra, John Wiley and Sons Ltd., Singapore.
(34) A. S. Khan, H. Khalid, Z. Sarfraz, M. Khan, J. Iqbal, N. Muhammad, M. A. Fareed, I. U. Rehman, Appl. Spectrosc. Rev. 2016, 52, 507. https://doi.org/10.1080/05704928.2016. 1244069
(35) N. Jidenko, J. P. Borra, J. Aerosol Sci. 2004, 35, 29. https://doi.org/10.1016/j.jaerosci.2004.06.013

(36) A. Bacher, Infrared Spectroscopy, University of California, Berkeley, CA 2002.
(37) G. Tillet, B. Boutevin, B. Ameduri, Prog. Polym. Sci. 2011, 36, 191. https://doi.org/10.1016/j.progpolymsci.2010.08.003
(38) A. Y. Arasi, J. J. Jeyakumari, B. Sundaresan, V. Dhanalakshmi, R. Anbarasan, Spectrochim. Acta A: Mol. Biomol. Spectrosc. 2009, 74, 1229. https://doi.org/10.1016/j.saa.2009.09.042